LETTERS

Prohibitin couples diapause signalling to mitochondrial metabolism during ageing in *C. elegans*

Marta Artal-Sanz[1] & Nektarios Tavernarakis[1]

Marked alterations in cellular energy metabolism are a universal hallmark of the ageing process[1]. The biogenesis and function of mitochondria, the energy-generating organelles in eukaryotic cells, are primary longevity determinants. Genetic or pharmacological manipulations of mitochondrial activity profoundly affect the lifespan of diverse organisms[2]. However, the molecular mechanisms regulating mitochondrial biogenesis and energy metabolism during ageing are poorly understood. Prohibitins are ubiquitous, evolutionarily conserved proteins, which form a ring-like, high-molecular-mass complex at the inner membrane of mitochondria[3]. Here, we show that the mitochondrial prohibitin complex promotes longevity by modulating mitochondrial function and fat metabolism in the nematode *Caenorhabditis elegans*. We found that prohibitin deficiency shortens the lifespan of otherwise wild-type animals. Notably, knockdown of prohibitin promotes longevity in diapause mutants or under conditions of dietary restriction. In addition, prohibitin deficiency extends the lifespan of animals with compromised mitochondrial function or fat metabolism. Depletion of prohibitin influences ATP levels, animal fat content and mitochondrial proliferation in a genetic-background- and age-specific manner. Together, these findings reveal a novel mechanism regulating mitochondrial biogenesis and function, with opposing effects on energy metabolism, fat utilization and ageing in *C. elegans*. Prohibitin may have a similar key role in modulating energy metabolism during ageing in mammals.

The mitochondrial prohibitin complex comprises two subunits (PHB-1 and PHB-2) that assemble at the inner mitochondrial membrane[4]. Prohibitins have been implicated in several important cellular processes such as mitochondrial biogenesis and function, signalling, transcriptional control, cell death and replicative senescence. In addition, prohibitins have been associated with various types of cancer (reviewed in ref. 5). Little is known about the role of prohibitin in chronological ageing. We examined the requirement for prohibitin during ageing in *C. elegans*. Prohibitin genes are widely expressed in animal tissues throughout development and during adulthood. Green fluorescent protein (GFP)-tagged PHB-1 and -2 co-localize in mitochondria (Supplementary Fig. 1; ref. 6). Elimination of either PHB-1 or PHB-2 by RNA interference (RNAi; Supplementary Fig. 2) disrupts the mitochondrial prohibitin complex and causes early embryonic lethality[6]. Homozygous mutants harbouring a null *phb-1* allele become gametogenesis-defective sterile adults due to maternal effect (see Methods).

Post-embryonic RNAi knockdown of either *phb-1* or *phb-2* shortens the lifespan of otherwise wild-type worms (Fig. 1a and Supplementary Table 1). In sharp contrast, prohibitin deficiency markedly extends the lifespan of long-lived *daf-2* mutants (Fig. 1b and Supplementary Table 1. The insulin/insulin-like growth factor (IGF) receptor DAF-2 is a component of a signalling pathway regulating diapause entry (dauer larva formation)[7]. Longevity conferred by *daf-2* mutations requires the DAF-16/FOXO transcription factor (reviewed in ref. 8). Loss of DAF-16 fully suppresses the exceptional longevity of prohibitin-depleted, *daf-2* mutants (Fig. 1c and Supplementary Table 1).

The transforming growth factor-β (TGF-β) signal transduction pathway also controls diapause and ageing[9]. The *daf-7* and *daf-4* genes encode a TGF-β homologue and the type II, transmembrane TGF-β receptor serine/threonine kinase, respectively[10,11]. Prohibitin depletion

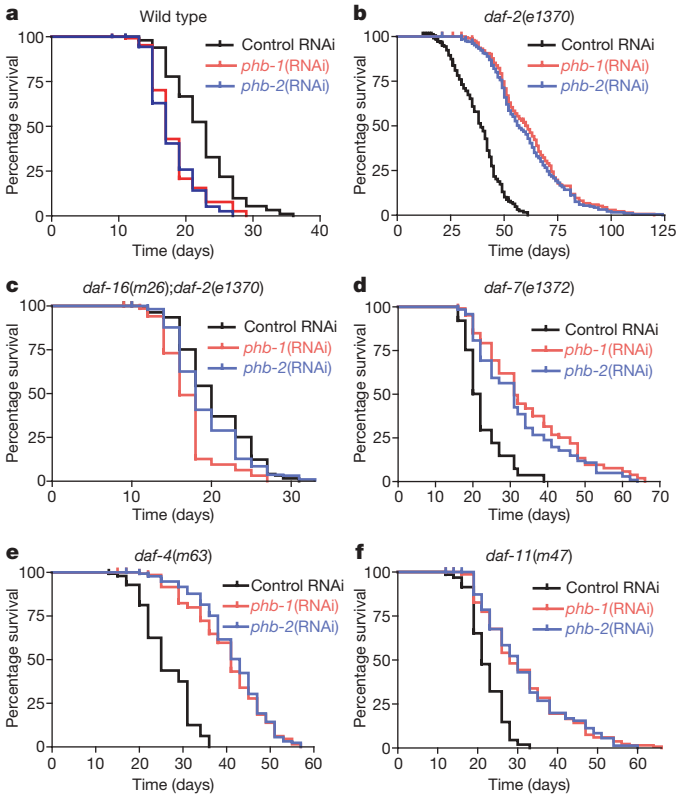

Figure 1 | Prohibitin deficiency markedly extends the lifespan of dauer-defective *C. elegans* mutants while shortening the lifespan of otherwise wild-type animals. The percentage of animals remaining alive is plotted against animal age. Assays were carried out at 20 °C. Combined lifespan data from independent experiments are given in Supplementary Table 1. **a**, Depletion of either PHB-1 or PHB-2 by RNAi in wild-type (N2) animals shortens lifespan. **b**, Prohibitin knockdown further extends the lifespan of long-lived, insulin signalling-defective *daf-2*(*e1370*) mutant animals. **c**, The longevity of prohibitin-depleted, *daf-2*(*e1370*) mutants is dependent on the transcription factor DAF-16/FOXO. **d**, Knockdown of either the *phb-1* or the *phb-2* gene extends the lifespan of *daf-7*(*e1372*) mutant animals, defective in TGF-β signalling. **e**, Survival curves of dauer-defective *daf-4* mutants subjected to RNAi with either *phb-1* or *phb-2*. **f**, Survival curves of dauer-defective *daf-11* mutants subjected to RNAi with either *phb-1* or *phb-2*.

[1]Institute of Molecular Biology and Biotechnology, Foundation for Research and Technology, Heraklion 71110, Crete, Greece.

extends the lifespan of both *daf-7* and *daf-4* mutant animals (Fig. 1d, e and Supplementary Table 1). Furthermore, knockdown of *phb-1* or *phb-2* extends the lifespan of animals carrying a lesion in the *daf-11* gene, which encodes a transmembrane guanylate cyclase that functions via both the insulin/IGF and the TGF-β pathways to modulate dauer formation[12] (Fig. 1f and Supplementary Table 1). Thus, depending on the genetic background, prohibitin function has opposing effects on *C. elegans* ageing. Although depletion of prohibitin compromises survival in wild-type animals, it substantially extends the lifespan of mutants defective in either of the two diapause signalling pathways.

Both PHB-1 and PHB-2 proteins localize in mitochondria, where they form a high-molecular-mass complex (Supplementary Fig. 1; ref. 6). We investigated the role of prohibitin during ageing in animals carrying mutations that affect the mitochondrial electron transport chain. Knockdown of *phb-1* or *phb-2* extends the lifespan of *gas-1* mutants (Fig. 2a and Supplementary Table 1). The *gas-1* gene encodes a homologue of the 49-kDa iron-sulphur subunit of the mitochondrial electron transport chain complex I. Similarly, prohibitin depletion extends the lifespan of nematodes with lesions in the *mev-1* and *isp-1* genes (Fig. 2b, c and Supplementary Table 1). *mev-1* and *isp-1* encode the succinate dehydrogenase cytochrome *b*, a component of complex II, and the Rieske iron-sulphur protein, a subunit of complex III, respectively. In addition, prohibitin knockdown extends the lifespan of *clk-1* mutant animals (Fig. 2d and Supplementary Table 1), which are defective in the biosynthesis of ubiquinone, an essential component of the electron transport chain. Hence, reduced prohibitin activity promotes survival of animals with compromised mitochondrial function. Energy metabolism in mitochondria is also affected by dietary restriction. We find that prohibitin deficiency improves the survival of dietary-restricted *eat-2* mutants (Fig. 2e and Supplementary Table 1).

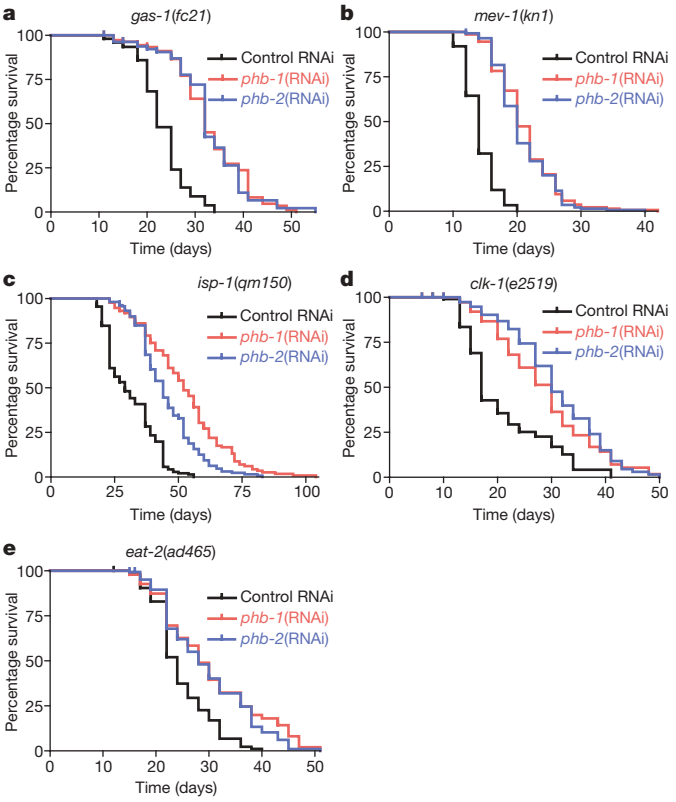

Figure 2 | Prohibitin deficiency further extends the lifespan of mitochondrial and dietary-restricted *C. elegans* mutants. Survival curves of mutant animal populations subjected to *phb-1* or *phb-2* RNAi are shown. **a**, Knockdown of prohibitin in mutants carrying a lesion in the *gas-1* gene, which encodes a homologue of the 49-kDa iron-sulphur protein fraction subunit of the mitochondrial NADH:ubiquinone-oxidoreductase, a component of the mitochondrial electron transport chain complex I. **b**, Knock-down of prohibitin in *mev-1* mutants, which lack succinate dehydrogenase cytochrome *b*, a component of the mitochondrial electron transport chain complex II. **c**, Knock-down of prohibitin in *isp-1* mutants, deficient for the Rieske iron-sulphur protein (ISP), a subunit of the mitochondrial electron transport chain complex III. **d**, Knock-down of prohibitin in long-lived animals carrying a mutation in the *clk-1* gene encoding a mitochondrial ubiquinone biosynthesis enzyme. **e**, Knock-down of prohibitin in long-lived, dietary-restricted *eat-2* mutants. The percentage of animals remaining alive is plotted against animal age. Lifespan values are given in Supplementary Table 1; assays were carried out at 20 °C.

To gain insight into the mechanism underlying the distinctive effects of prohibitin on ageing, we performed a temporal analysis of ATP levels during ageing (at day 3, 10 and 15 of adulthood) in wild-type animals and in *daf-2* and *daf-7* diapause mutants. We found that ATP levels are higher in diapause mutants compared to age-matched wild-type control animals. Knockdown of prohibitin specifically increased the levels of ATP in dauer-defective *daf-2* and *daf-7* mutants, progressively with age. In contrast, we did not detect ATP elevation in prohibitin-depleted wild-type animals during ageing (Fig. 3a; data for day 10 shown). The significant energy surplus in *daf-2* mutants lacking prohibitin correlates with their exceptionally long lifespan (Fig. 1b). Our findings indicate that prohibitin moderates ATP levels under conditions of reduced diapause signalling.

What is the molecular basis of the different impact of prohibitin on ATP levels between wild type and diapause mutant animals? Mitochondrial energy metabolism is linked to fat utilization in both nematodes and mammals. We visualized fat depositions in the intestine of wild-type animals and diapause mutants during ageing, using the vital dye Nile red (see Methods). Fat accumulates during ageing in wild-type animals and in two representative diapause mutants (*daf-2* and *daf-7*; Fig. 3b and Supplementary Fig. 3a). These observations were confirmed by Sudan black staining of fixed animals (Supplementary Fig. 3b). Prohibitin deficiency markedly reduces intestinal fat content early in adulthood, in all genetic backgrounds (Fig. 3b and Supplementary Fig. 3a, day 5). However, the effect of prohibitin depletion diminishes with age in wild-type animals, whereas it remains strong in both diapause mutants (Fig. 3b and Supplementary Fig. 3a, day 10 and day 15). Thus, prohibitin differentially modulates animal fat content in a genetic background- and age-specific manner.

The nuclear hormone receptor NHR-49 is a key regulator of fat mobilization, modulating fat consumption and maintaining a normal balance of fatty acid saturation. Elimination of NHR-49 causes fat accumulation due to reduced expression of fatty acid β-oxidation enzymes such as the delta-9 stearoyl-CoA desaturase FAT-7, which is required for the synthesis of monounsaturated fatty acids[13]. Prohibitin deficiency extends the lifespan of both *nhr-49* and *fat-7* mutants (Fig. 3c, d; Supplementary Table 1). In addition, knockdown of prohibitin reduces intestinal fat in *nhr-49* and *fat-7* mutant animals (Supplementary Fig. 4a, b). Taken together, our findings indicate that prohibitin deficiency engages fat metabolism to promote longevity.

Prohibitin has been implicated in several human cancers and is generally overexpressed in transformed cells compared with their non-transformed counterparts[5]. We examined the requirement for prohibitin activity during tumour formation in *C. elegans*. Although *C. elegans* somatic cells are post-mitotic, germ cells are continually dividing during oogenesis. *gld-1* is a tumour suppressor gene that encodes a protein containing a K homology RNA-binding domain that is required for meiotic cell cycle progression during oogenesis[14]. *gld-1* mutant animals develop lethal germline tumours and are short lived because of ectopic germ cell overproliferation in the gonad[14]. Germ cells eventually leak out of the gonad into the body cavity or, through the vulva, to the outside. We find that prohibitin deficiency blocks tumour formation and extends lifespan in *gld-1* mutants (compare Supplementary Fig. 5a with b; Supplementary Table 1). These observations indicate a critical function of prohibitin in actively proliferating cells[6,15,16].

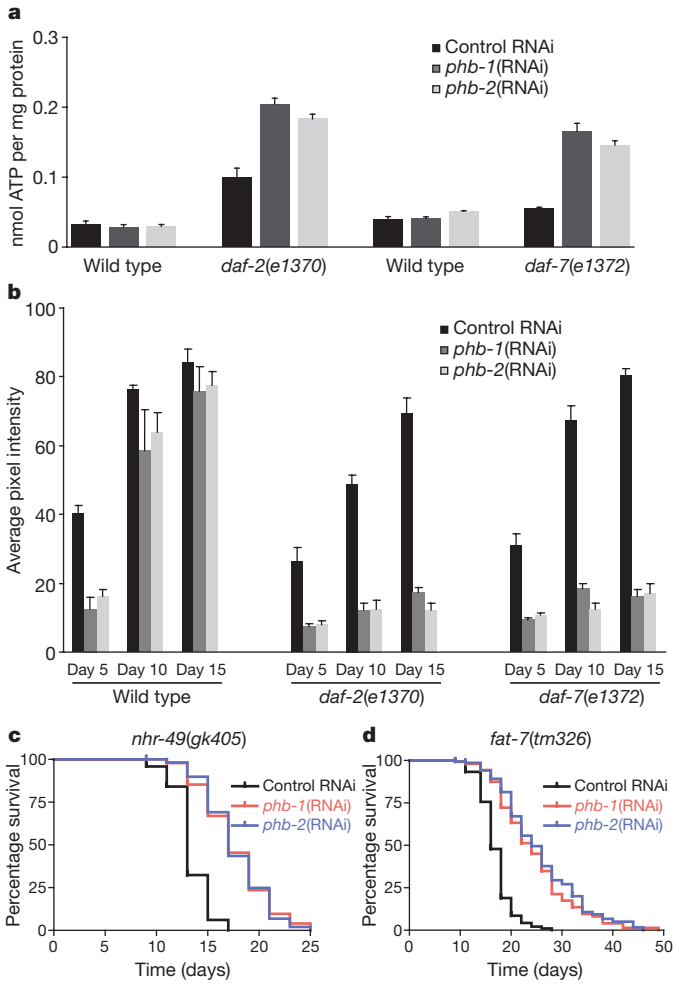

Figure 3 | Effects of prohibitin depletion on energy metabolism. a, RNAi knockdown of either *phb-1* or *phb-2* specifically increases ATP levels in dauer-defective *daf-2* or *daf-7* mutants during ageing (day 10 of adulthood). No effect is observed in wild-type (N2) animals (error bars denote standard deviation; $P < 0.005$, unpaired *t* test; assays were carried out at 20 °C). **b**, Quantification of intestinal fluorescence after Nile red staining of wild-type animals and dauer-defective mutants, subjected to RNAi with either *phb-1* or *phb-2* at day 5, day 10 and day 15 of adulthood (error bars denote standard deviation; $P < 0.005$, unpaired *t* test; assays were carried out at 20 °C; see Methods). **c**, **d**, Survival curves of short-lived *nhr-49* mutants (**c**) and animals lacking the delta-9 desaturase FAT-7 (**d**), subjected to RNAi with either *phb-1* or *phb-2*.

To investigate the mechanism by which prohibitin influences mitochondrial activity to modulate longevity, we analysed cellular mitochondrial content during ageing. We found that prohibitin elimination promotes adult-onset mitochondrial proliferation in intestinal fat-storing cells of wild-type animals whereas, strikingly, it reduces mitochondrial content in diapause mutants. Notably, these mutants contain less mitochondria compared to wild type, during late adulthood (Fig. 4a and Supplementary Fig. 6a, b). Mitochondrial and fat content is also reduced upon knockdown of *phb* genes in mutants with compromised mitochondrial function, in dietary restricted animals, and in fat metabolism mutants (Fig. 4b and Supplementary Fig. 7a). In *Drosophila* and in the adipose tissue of mice, FOXO transcription factors inhibit mitochondrial proliferation[17,18]. We observed a similar effect in *C. elegans* diapause mutants (Fig. 4a), where DAF-16/FOXO is derepressed[9]. In contrast, prohibitin depletion does not significantly alter fat or mitochondrial content in animals lacking DAF-16 ($P > 0.1$, unpaired *t* test; Supplementary Fig. 8a). Hence, DAF-16 is required to mediate the effects of prohibitin deficiency on fat and mitochondrial content in wild-type animals. However, elimination of prohibitin during adulthood does not affect the subcellular localization of either a wild-type or a constitutively nuclear DAF-16 reporter fusion (Supplementary Fig. 8b). In addition, constitutive nuclear localization of DAF-16 is not sufficient to extend the lifespan of prohibitin-depleted animals (Supplementary Table 1). Moreover, the ageing effects of knockout or overexpression of sirtuin SIR-2.1, a regulator of DAF-16, are independent of prohibitin (Supplementary Table 1).

Together, our findings show a new mechanism that couples nutrient availability and diapause signals with energy metabolism during ageing. We hypothesize that prohibitin normally functions to promote longevity by moderating fat utilization and energy production via the mitochondrial respiratory chain. Under conditions that favour diapause, such as limited nutrient availability, cells adapt by shifting towards fermentative metabolism[19]. Under such conditions, when energy demands exceed the capacity of mitochondrial respiration, prohibitin deficiency is beneficial for survival. We tested this hypothesis by monitoring survival of animals lacking prohibitin at a higher temperature (25 °C), where metabolic activity is elevated and energy demand is higher. Notably, whereas knockdown of prohibitin shortens lifespan at 20 °C it extends lifespan at 25 °C (Supplementary Table 1). We also tested the requirement for prohibitin under acute thermal stress (35 °C). Prohibitin deficiency renders wild-type animals strongly thermotolerant and further enhances the thermotolerance of *daf-2* diapause mutants (Supplementary Fig. 9a, b). Thus, the metabolic state determines whether prohibitin will promote or compromise longevity. Increased thermotolerance is independent of DAF-16/FOXO (Supplementary Fig. 8c), indicating that other pathways are involved in metabolic changes elicited by prohibitin deficiency.

We also examined the effects of prohibitin depletion on animals under oxidative stress. We induced oxidative stress by using sodium azide (NaN_3), a potent and specific inhibitor of cytochrome *c* oxidase, a component of the mitochondrial electron transport chain complex IV. Prohibitin depletion enhances survival after treatment with sodium azide during adulthood in diapause mutants (Supplementary Fig. 9c). Similarly, prohibitin deficiency increases resistance of adult *daf-2* mutant animals to the herbicide paraquat (*N*,*N*′-dimethyl-4,4′-bipyridinium dichloride), a generator of superoxide anions (Supplementary Fig. 9d). By contrast, lack of prohibitin compromises paraquat resistance during adulthood in an otherwise wild-type genetic background and during L4 larval development in both wild-type and *daf-2* mutant animals (Supplementary Fig. 9e, f; ref. 6). Therefore, elimination of prohibitin under conditions of reduced diapause signalling further increases oxidative stress resistance during adulthood. We conclude that lack of prohibitin diminishes mitochondrial proliferation during ageing, augments oxidative stress resistance and extends lifespan, specifically under conditions of reduced insulin/IGF and TGF-β signalling.

Mitochondria are the main sites of reactive oxygen species generation within cells. We measured reactive oxygen species formation upon prohibitin depletion in both wild-type and *daf-2* mutant adult animals under normal and oxidative stress conditions. Reactive oxygen species levels were slightly lower in *daf-2* mutants compared to wild type (Supplementary Fig. 9g). Notably, although prohibitin deficiency increased reactive oxygen species formation in wild-type animals, it reduced reactive oxygen species levels in *daf-2* mutant adults (Supplementary Fig. 9g). We also assessed mitochondrial membrane potential and oxygen consumption in prohibitin-deficient, wild-type and *daf-2* mutant animals. Knockdown of prohibitin slightly reduces mitochondrial membrane potential, while selectively increasing oxygen consumption in *daf-2* mutants (Supplementary Fig. 10a, b). Paradoxically, reactive oxygen species formation has been shown to underlie oxidative stress resistance and lifespan extension under glucose restriction in *C. elegans*[20]. It has been suggested that stress resistance and longevity are due to induction of a hormetic response (mitohormesis)[20]. We investigated whether increased reactive oxygen species formation augments stress resistance and extends lifespan in prohibitin-deficient animals under stress. We treated prohibitin-depleted

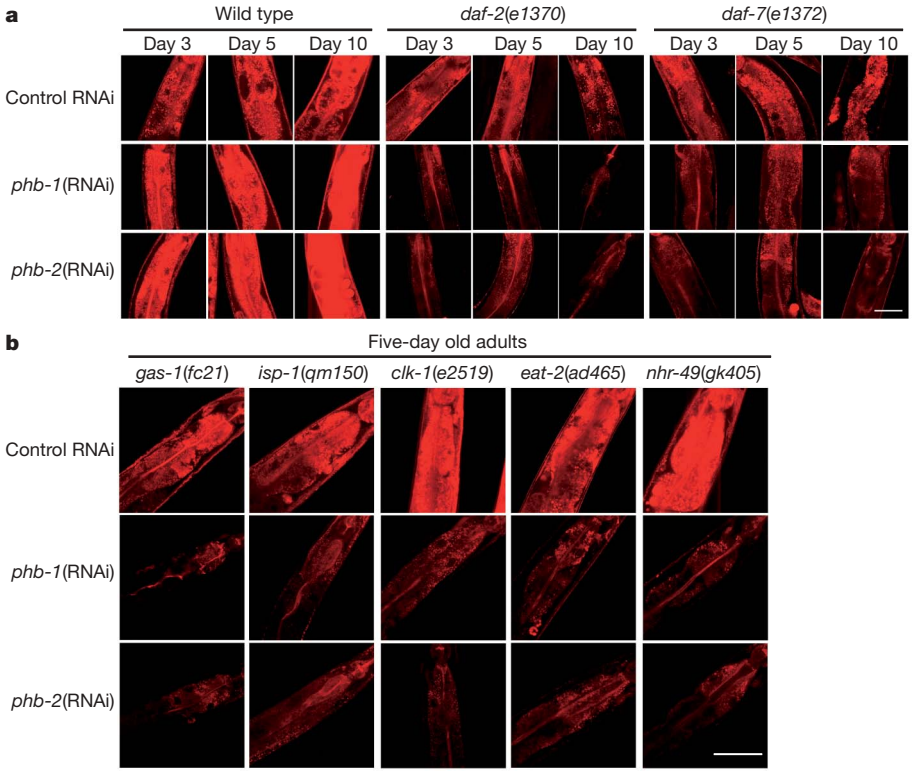

Figure 4 | Prohibitin depletion and intestinal fat-storing cell mitochondrial content. a, MitoTracker Deep Red 633 staining of intestinal mitochondria in wild-type animals and dauer-defective *daf-2* or *daf-7* mutants subjected to RNAi with either *phb-1* or *phb-2*. Images were acquired under the same exposure, using a ×40 objective lens, at day 3, day 5 and day 10 of adulthood (see Methods; the anterior part of the intestine is shown, the head is located at the top; bar, 50 μm). **b**, MitoTracker Deep Red 633 staining of intestinal mitochondria in *gas-1*(*fc21*), *isp-1*(*qm150*), *clk-1*(*e2519*), *eat-2*(*ad465*) and *nhr-49*(*gk405*) mutants subjected to RNAi with either *phb-1* or *phb-2*. Images were acquired under the same exposure, using a ×40 objective lens at day 5 of adulthood.

animals experiencing either oxidative stress (*mev-1* mutants) or thermal stress (wild-type nematodes grown at 25 °C) with *N*-acetylcysteine, a compound that functions as a free-radical scavenger[20]. We found no effect on longevity conferred by prohibitin knockdown (Supplementary Table 1 and Supplementary Fig. 11). Thus mitohormesis is unlikely to mediate the effects of prohibitin elimination on ageing.

The AMP-dependent kinase (AMPK) AAK-2 has been implicated in coupling energy levels and insulin/IGF-1 signals to modulate lifespan in *C. elegans*[20,21]. AMPK targets p53 to promote cell survival under conditions of nutrient deprivation[22]. We find that prohibitin deficiency shortens the lifespan of both *aak-2* and p53 (*cep-1*) mutant animals (Supplementary Table 1 and Supplementary Fig. 12a, b). Interestingly, *aak-2* mutants contain more mitochondria than wild-type animals. Depletion of prohibitins further increases mitochondrial proliferation in this genetic background (Supplementary Fig. 12c, d). In addition, AAK-2 deficiency ameliorates fat content reduction upon prohibitin depletion (Supplementary Fig. 12e, f), indicating that AAK-2 is involved in mediating prohibitin effects on fat content. We also investigated the involvement of the mitogen-activated protein kinase (MAPK) JNK-1, which promotes DAF-16/FOXO nuclear localization under conditions of stress[23], and the Akt/PKB homologue AKT-1, which transduces insulin/IGF-1 signals[24], in mediating the effects of prohibitin depletion on metabolism and ageing. We found that *phb* gene knockdown marginally extends the lifespan of animals overexpressing *jnk-1*, whereas it shortens lifespan in animals lacking JNK-1 (Supplementary Table 1 and Supplementary Fig. 13a). Overexpression of JNK-1 in wild-type animals reduces mitochondrial content and suppresses mitochondrial proliferation upon prohibitin depletion. By contrast, mitochondrial content is higher in *jnk-1* mutants and remains unchanged after prohibitin removal (Supplementary Fig. 13b, c). Similarly, prohibitin deficiency does not alter fat content in *jnk-1* mutant animals (Supplementary Fig. 13d, e). Thus, JNK-1 is required for mitochondrial proliferation and reduction of fat content in animals lacking prohibitin. Elimination of prohibitin does not shorten the lifespan of animals without AKT-1 (Supplementary Table 1 and Supplementary Fig. 13a). Mitochondrial content is reduced in *akt-1* mutants and does not increase upon prohibitin depletion, compared to wild type (Supplementary Fig. 13b, c). In contrast, fat content in *akt-1* mutants is higher than in wild type and sharply diminishes in the absence of prohibitin, similarly to *daf-2* mutant animals (Supplementary Fig. 13d, e). Taken together, our observations indicate that the JNK-1 kinase, in part, mediates the effects of prohibitin deficiency on fat metabolism and mitochondrial proliferation. This response is potentiated under conditions of low diapause signalling, where AKT-1 activity is reduced and DAF-16/FOXO nuclear localization is not blocked.

In mammalian cells and in *C. elegans*, loss of prohibitin disrupts the reticular mitochondrial network and leads to accumulation of fragmented mitochondria[6,25]. Prohibitin maintains mitochondrial integrity and biogenesis by stabilizing the dynamin-like GTPase OPA1[25], a core component of the mitochondrial fusion machinery, which is required for mitochondrial fusion and cristae maintenance, and has been implicated in the pathogenesis of inherited autosomal dominant optic atrophy[26]. The *eat-3* gene encodes the *C. elegans* homologue of OPA1. We examined whether prohibitin functions through OPA1 to regulate metabolism during ageing, by analysing the effects of EAT-3 depletion on fat metabolism, mitochondrial content, ATP levels and lifespan, in wild type and insulin/IGF1 signalling-deficient animals. In contrast to prohibitin depletion, loss of EAT-3 extends the lifespan of otherwise wild-type animals, whereas it shortens the lifespan of long-lived *daf-2* mutants (Supplementary Table 1 and Supplementary Fig. 14a, b). We did not observe significant alterations of fat metabolism, ATP levels or mitochondrial content in

EAT-3-deficient animals (Supplementary Fig. 14c–e). Our findings indicate that prohibitin functions independently of EAT-3/OPA1 to regulate metabolism during ageing.

What is the origin of prohibitin effects on metabolism and ageing? We propose that under normal conditions the mitochondrial prohibitin complex promotes longevity by moderating fat metabolism, mitochondrial proliferation and energy levels in *C. elegans*. In addition to maintaining normal mitochondrial metabolism, prohibitin functions as a negative regulator of mitochondrial proliferation in wild-type animals (Supplementary Fig. 15). Elimination of prohibitin may activate a cellular retrograde response that induces mitochondrial overproliferation. In turn, accumulation of defective mitochondria lacking prohibitin results in increased reactive oxygen species production, metabolic defects, consequent cellular damage and reduced lifespan. Interestingly, prohibitin depletion elicits reactive-oxygen-species-dependent, Akt hyperactivation in endothelial cells[27]. Under low diapause signalling and stress conditions, where AKT-1-mediated inhibition of DAF-16/FOXO nuclear localization is relieved, the JNK-1 and AAK-2 stress-related signalling pathways are activated by prohibitin depletion, adjusting cellular metabolism towards fat utilization and promoting longevity.

Our study reveals an important role of prohibitin in regulating fat metabolism and mitochondrial proliferation during ageing. The opposing effects of prohibitin on longevity indicate that specific cellular mechanisms may differentially regulate ageing, depending on extrinsic or intrinsic cues such as diapause signalling or energy demands. The tight evolutionary conservation and ubiquitous expression of prohibitin proteins indicate a similar role during ageing in other organisms.

METHODS SUMMARY

Lifespan analysis. Lifespan assays were performed at 20 °C unless noted otherwise. Synchronous animal populations were generated by hypochlorite treatment of gravid adults to obtain tightly synchronized embryos that were allowed to develop into adulthood under appropriate, defined conditions. Animals were transferred to fresh plates in groups of 10–20 worms per plate for a total of 100–150 individuals per experiment. The day of egg harvest was used as $t = 0$. Animals were transferred to fresh plates every 2–4 days thereafter and were examined every day for touch-provoked movement and pharyngeal pumping, until death. Survival curves were generated using the product-limit method of Kaplan and Meier. The log-rank (Mantel–Cox) test was used to evaluate differences in survival and determine P values.

MitoTracker staining. Animals were stained overnight on plates containing MitoTracker Deep Red 633 at a final concentration of 100 nM. Animals were mounted on 2% agarose pads in M9 buffer containing 10 mM sodium azide and scanned at room temperature with a 637 nm laser beam, under a confocal microscope.

Full Methods and any associated references are available in the online version of the paper at www.nature.com/nature.

Received 10 July; accepted 24 August 2009.

1. Roberts, S. B. & Rosenberg, I. Nutrition and aging: changes in the regulation of energy metabolism with aging. *Physiol. Rev.* **86,** 651–667 (2006).
2. Balaban, R. S., Nemoto, S. & Finkel, T. Mitochondria, oxidants, and aging. *Cell* **120,** 483–495 (2005).
3. Back, J. W. *et al.* A structure for the yeast prohibitin complex: structure prediction and evidence from chemical crosslinking and mass spectrometry. *Protein Sci.* **11,** 2471–2478 (2002).
4. Nijtmans, L. G. *et al.* Prohibitins act as a membrane-bound chaperone for the stabilization of mitochondrial proteins. *EMBO J.* **19,** 2444–2451 (2000).
5. Mishra, S., Murphy, L. C., Nyomba, B. L. & Murphy, L. J. Prohibitin: a potential target for new therapeutics. *Trends Mol. Med.* **11,** 192–197 (2005).
6. Artal-Sanz, M. *et al.* The mitochondrial prohibitin complex is essential for embryonic viability and germline function in *Caenorhabditis elegans*. *J. Biol. Chem.* **278,** 32091–32099 (2003).
7. Kimura, K. D., Tissenbaum, H. A., Liu, Y. & Ruvkun, G. *daf-2*, an insulin receptor-like gene that regulates longevity and diapause in *Caenorhabditis elegans*. *Science* **277,** 942–946 (1997).
8. Kenyon, C. The plasticity of aging: insights from long-lived mutants. *Cell* **120,** 449–460 (2005).
9. Shaw, W. M. *et al.* The *C. elegans* TGF-β dauer pathway regulates longevity via insulin signaling. *Curr. Biol.* **17,** 1635–1645 (2007).
10. Estevez, M. *et al.* The *daf-4* gene encodes a bone morphogenetic protein receptor controlling *C. elegans* dauer larva development. *Nature* **365,** 644–649 (1993).
11. Ren, P. *et al.* Control of *C. elegans* larval development by neuronal expression of a TGF-β homolog. *Science* **274,** 1389–1391 (1996).
12. Li, W., Kennedy, S. G. & Ruvkun, G. *daf-28* encodes a *C. elegans* insulin superfamily member that is regulated by environmental cues and acts in the DAF-2 signaling pathway. *Genes Dev.* **17,** 844–858 (2003).
13. Van Gilst, M. R., Hadjivassiliou, H., Jolly, A. & Yamamoto, K. R. Nuclear hormone receptor NHR-49 controls fat consumption and fatty acid composition in *C. elegans*. *PLoS Biol.* **3,** e53 (2005).
14. Francis, R., Barton, M. K., Kimble, J. & Schedl, T. *gld-1*, a tumor suppressor gene required for oocyte development in *Caenorhabditis elegans*. *Genetics* **139,** 579–606 (1995).
15. Coates, P. J., Jamieson, D. J., Smart, K., Prescott, A. R. & Hall, P. A. The prohibitin family of mitochondrial proteins regulate replicative lifespan. *Curr. Biol.* **7,** 607–610 (1997).
16. Coates, P. J. *et al.* Mammalian prohibitin proteins respond to mitochondrial stress and decrease during cellular senescence. *Exp. Cell Res.* **265,** 262–273 (2001).
17. Gershman, B. *et al.* High-resolution dynamics of the transcriptional response to nutrition in *Drosophila*: a key role for dFOXO. *Physiol. Genom.* **29,** 24–34 (2007).
18. Nakae, J. *et al.* Forkhead transcription factor FoxO1 in adipose tissues regulates energy storage and expenditure. *Diabetes* **57,** 563–576 (2008).
19. Rea, S. & Johnson, T. E. A metabolic model for life span determination in *Caenorhabditis elegans*. *Dev. Cell* **5,** 197–203 (2003).
20. Schulz, T. J. *et al.* Glucose restriction extends *Caenorhabditis elegans* life span by inducing mitochondrial respiration and increasing oxidative stress. *Cell Metab.* **6,** 280–293 (2007).
21. Apfeld, J., O'Connor, G., McDonagh, T., DiStefano, P. S. & Curtis, R. The AMP-activated protein kinase AAK-2 links energy levels and insulin-like signals to lifespan in *C. elegans*. *Genes Dev.* **18,** 3004–3009 (2004).
22. Jones, R. G. *et al.* AMP-activated protein kinase induces a p53-dependent metabolic checkpoint. *Mol. Cell* **18,** 283–293 (2005).
23. Oh, S. W. *et al.* JNK regulates lifespan in *Caenorhabditis elegans* by modulating nuclear translocation of forkhead transcription factor/DAF-16. *Proc. Natl Acad. Sci. USA* **102,** 4494–4499 (2005).
24. Paradis, S. & Ruvkun, G. *Caenorhabditis elegans* Akt/PKB transduces insulin receptor-like signals from AGE-1 PI3 kinase to the DAF-16 transcription factor. *Genes Dev.* **12,** 2488–2498 (1998).
25. Merkwirth, C. *et al.* Prohibitins control cell proliferation and apoptosis by regulating OPA1-dependent cristae morphogenesis in mitochondria. *Genes Dev.* **22,** 476–488 (2008).
26. Olichon, A. *et al.* Loss of OPA1 perturbates the mitochondrial inner membrane structure and integrity, leading to cytochrome c release and apoptosis. *J. Biol. Chem.* **278,** 7743–7746 (2003).
27. Schleicher, M. *et al.* Prohibitin-1 maintains the angiogenic capacity of endothelial cells by regulating mitochondrial function and senescence. *J. Cell Biol.* **180,** 101–112 (2008).

Supplementary Information is linked to the online version of the paper at www.nature.com/nature.

Acknowledgements We thank A. Pasparaki for technical support with experiments. Some nematode strains used in this work were provided by the *C. elegans* Gene Knockout Project at OMRF (http://www.mutantfactory.ouhsc.edu/), which is part of the International *C. elegans* Gene Knockout Consortium, the *Caenorhabditis* Genetics Center, which is funded by the NIH National Center for Research Resources (NCRR), and S. Mitani (National Bioresource Project) in Japan. We thank A. Fire for plasmid vectors and J. Berden for antibodies. This work was funded by grants from EMBO, the European Research Council (ERC), the Marie Curie Fellowships Programme and the European Commission Coordination Action ENINET (contract number LSHM-CT-2005-19063).

Author Contributions M.A.-S. and N.T. designed and performed experiments, analysed data and wrote the manuscript.

Author Information Reprints and permissions information is available at www.nature.com/reprints. Correspondence and requests for materials should be addressed to N.T. (tavernarakis@imbb.forth.gr) or M.A.-S. (martal@ibv.csic.es).

METHODS

Strains and genetics. We followed standard procedures for *C. elegans* strain maintenance. Nematode rearing temperature was kept at 20 °C, unless noted otherwise. The following strains were used in this study: N2, wild-type Bristol isolate; CB1370, *daf-2*(*e1370*)*III*; CB1372, *daf-7*(*e1372*)*III*, CB4876: *clk-1*(*e2519*)*III*, CF1139: *daf-16*(*mu86*)*I*;*muIs61*, CF1308: *daf-16*(*mu86*)*I*;*muEx116*, CF1371: *daf-16*(*mu86*)*I*;*muEx151*, CW152: *gas-1*(*fc21*)*X*, DA465: *eat-2*(*ad465*)*II*, DR26: *daf-16*(*m26*)*I*, DR47: *daf-11*(*m47*)*V*, DR63: *daf-4*(*m63*)*III*, DR1309: *daf-16*(*m26*)*I*;*daf-2*(*e1370*)*II*, GR1307: *daf-16*(*mgDf50*)*I*, HT941: *lpIn1*, JK1466: *gld-1*(*q485*)*/dpy-5*(*e61*) *unc-13*(*e51*)*I*, LG100: *geIn3*; MQ887: *isp-1*(*qm150*)*IV*, RB754: *aak-2*(*ok524*)*X*, RB759: *akt-1*(*ok525*)*V*, TK22: *mev-1*(*kn1*)*III*, VC8: *jnk-1*(*gk7*)*IV*, VC199: *sir-2.1*(*ok434*)*IV*, VC870: *nhr-49*(*gk405*)*I*;*fat-7*(*tm0326*), XY1054: *cep-1*(*lg12501*)*I*, N2*Ex*[$p_{phb\text{-}1}$PHB-1::GFP pRF4], N2*Ex*[$p_{phb\text{-}2}$PHB-2::GFP pRF4] and *phb-1*(*tm2571*)*I*;*sDp2*(*I*;*f*). The *sDp2*(*I*;*f*) balancer chromosomal duplication is unstable during meiosis and is lost in about 30% of the progeny, which become sterile homozygous *phb-1*(*tm2571*) adults.

Molecular cloning. For engineering *phb-1* and *phb-2* dsRNA-producing *Escherichia coli* bacteria, the corresponding genomic DNA fragments, previously inserted into the pBluescript II plasmid vector[6], were excised by SacI/KpnI and KpnI/SpeI, respectively, and sub-cloned into the pL4440 RNAi vector. The resulting plasmid construct was used to transform HT115(DE3) *E. coli* bacteria, deficient for RNase-E. Bacteria carrying an empty vector were used in control experiments. To generate $p_{phb\text{-}1}$PHB-1::GFP and $p_{phb\text{-}2}$PHB-2::GFP full-length GFP reporter fusions, DNA fragments derived from the *phb-1* and *phb-2* loci were PCR-amplified using appropriate oligonucleotide primers and fused to GFP. For $p_{phb\text{-}1}$PHB-1::GFP, the primers 5′-AACTGCAGCTCAACGCGTGAG CCATACC-3′ and 5′-GCTCTAGAGGATTGAAGGTTGAGAAGG-3′ were used to amplify a 1.7 kb DNA fragment encompassing the promoter plus the full coding region of *phb-1*, which was digested with PstI/XbaI and inserted into plasmid vector pPD95.77. Similarly, for $p_{phb\text{-}2}$PHB-2::GFP, the primers 5′-AC ATGCATGCGAGTCAGAGATAAAGACCG-3′ and 5′-GCTCTAGAGCGTCTT TTGTCGGTCAC-3′ were used to amplify a 1.9 kb DNA fragment encompassing the promoter plus the full coding region of *phb-2*, which was digested with SphI/XbaI and inserted into pPD95.77. Reporter constructs were injected into the gonads of wild-type animals together with pRF4, a plasmid that carries the *rol-6*(*su1006*) dominant transformation marker. Two independent, transgenic lines were obtained for the $p_{phb\text{-}1}$PHB-1::GFP plasmid construct and roller hermaphrodites were examined for reporter fusion expression. For $p_{phb\text{-}2}$PHB-2::GFP, we obtained and examined numerous (>50) F1 transgenic progeny, none of which propagated to generate a stable transgenic line, probably because the GFP moiety of the fusion interferes with the formation of the complex[28]. Transgenic animals were mounted on a 2% agarose pad in M9 buffer, containing 10 mM sodium azide and scanned at room temperature with a 488 nm laser beam, under a confocal microscope (Zeiss AxioScope with a Bio-Rad Radiance 2100 scanhead). Images were acquired using a 515 ± 15 nm band-pass filter and a ×40 Plan-NEOFLUAR objective (numerical aperture 0.75).

Lifespan analysis. Lifespan assays were performed at 20 °C unless noted otherwise. Synchronous animal populations were generated by hypochlorite treatment of gravid adults to obtain tightly synchronized embryos that were allowed to develop into adulthood under appropriate, defined conditions. For RNAi lifespan experiments worms were placed on NGM plates containing 1–2 mM IPTG and seeded with HT115(DE3) bacteria transformed with either the pL4440 vector or the test RNAi construct. Progeny were grown at 20 °C unless noted otherwise, through the L4 larval stage and then transferred to fresh plates in groups of 10–20 worms per plate for a total of 100–150 individuals per experiment. The day of egg harvest and initiation of RNAi was used as $t = 0$. Animals were transferred to fresh plates every 2–4 days thereafter and were examined every day for touch-provoked movement and pharyngeal pumping, until death. Worms that died due to internally hatched eggs, an extruded gonad or desiccation due to crawling on the edge of the plates, were censored and incorporated as such into the data set. Each survival assay was repeated at least three times and figures represent typical assays. Survival curves were created using the product-limit method of Kaplan and Meier. The log-rank (Mantel–Cox) test was used to evaluate differences between survivals and determine *P* values. We used the Prism software package (GraphPad Software) to carry out statistical analysis and to determine lifespan values.

Stress resistance assays. To evaluate thermotolerance, four-day-old adult hermaphrodites were placed on pre-warmed (35 °C) NGM plates and incubated at 35 °C. At the indicated times, plates were removed and worms were scored for motility, provoked movement and pharyngeal pumping. Worms failing to display any of these traits were scored as dead. Three distinct populations of 30 adults were scored repeatedly over the assay period. Statistical tests were performed using the Kaplan–Meier survival analysis, as described above for lifespan data. To analyse oxidative stress resistance, 7-day-old adults were exposed to 1 mM sodium azide (Sigma-Aldrich) for 18 h, on RNAi plates, at 20 °C. Animals were scored for survival after a 3-h recovery period. To assay paraquat resistance, 7-day-old adults were exposed to 40 mM paraquat (Aldrich) on RNAi plates at 20 °C and survival was scored from day 8 of adulthood. For paraquat resistance of L4 larvae, animals were exposed to 2 mM paraquat on RNAi plates at 20 °C and survival was scored every 2 days. The percentage of surviving animals for each drug treatment was calculated in three independent experiments. In each experiment, 100 animals were analysed. Statistical analysis of data was performed using the Excel software package (Microsoft).

Fat staining. Nile red powder (catalogue number N3013, Sigma-Aldrich) was dissolved in DMSO at 5 mg ml^{-1}, diluted in M9 and added on top of nematode growth media (NGM) plates seeded with HT115(DE3) *E. coli* bacteria harbouring the appropriate RNAi plasmids, to a final concentration of 0.02 μg ml^{-1}. Synchronous embryos were allowed to develop into adulthood and grow continuously on Nile red-containing plates. The extent of fat staining was assessed at specific time points by epifluorescence microscopy[29]. Animals were observed using a ×20 Plan-NEOFLUAR objective (numerical aperture 0.50), coupled with a 546 ± 12 nm band-pass excitation and a 590 nm long-pass emission filter, on a Zeiss AxioPlan microscope (Carl Zeiss). Images were acquired using a Zeiss AxioCam digital colour camera. Emission intensity was measured on greyscale images with a pixel depth of 8 bit (256 shades of grey). Average pixel intensity values were calculated by sampling three images of different animals, three times each (nine measurements total for each strain/condition). We calculated the mean and maximum pixel intensity for each animal in these images using the ImageJ software (http://rsb.info.nih.gov/ij/). For each experiment, at least 50 images were processed over at least five independent trials. Because recent studies suggested that Nile red may not accurately indicate fat content in insulin/IGF-1 mutants, owing to uptake and/or anatomical issues[30], animals were also stained with Sudan black (Sigma-Aldrich) as described previously[7]. Briefly, non-starved animals were collected in M9 buffer and washed three times. Animals were then fixed by adding 10% paraformaldehyde solution to final concentration of 1%. Fixed animals were frozen at −80 °C and underwent three cycles of freeze–thawing before washing in cold M9 buffer three times. Animals were subsequently dehydrated by ethanol washes (serially in 25%, 50% and 70% ethanol). For staining, three volumes of saturated Sudan black B solution (in 70% ethanol) were added to worms. Animals were incubated overnight and washed thrice with 70% ethanol before observation. Animals were observed using a ×20 Plan-NEOFLUAR objective (numerical aperture 0.50) on a Zeiss AxioPlan microscope (Carl Zeiss). Images were acquired using a Zeiss AxioCam digital camera. Emission intensity was measured on greyscale images with a pixel depth of 8 bit (256 shades of grey). Average pixel intensity values were calculated by sampling three images of different animals, three times each (nine measurements total for each strain). We calculated the mean and maximum pixel intensity for each animal in these images using the ImageJ software (http://rsb.info.nih.gov/ij/). Numbers obtained were subtracted from 255 to obtain the values depicted in Supplementary Fig. 3. For each experiment, at least 20 images were processed over at least three independent trials.

MitoTracker staining. Animals were stained overnight on RNAi plates containing MitoTracker Deep Red 633 (catalogue number M-22426; Molecular Probes, Invitrogen) at a final concentration of 100 nM. Animals were mounted in a 2% agarose pad in M9 buffer containing 10 mM sodium azide and scanned at room temperature with a 637 nm laser beam, under a confocal microscope (Zeiss AxioPlan coupled to a Bio-Rad Radiance 2000 laser scanning system). Images of emission were acquired using a 660 nm long-pass filter and a ×40 Plan-NEOFLUAR objective (NA 0.75), and processed with Bio-Rad LaserSharp 2000 software.

ATP measurements. To determine ATP content, 50 age-matched animals were collected in 50 μl of S Basal buffer and frozen at −80 °C. Nematodes were collected at the L4 stage of development and on day 2, day 10 and day 15 of adulthood. Frozen worms were immersed in boiling water for 15 min, cooled and centrifuged to pellet insoluble debris. The supernatant was moved to a fresh tube and diluted tenfold before measurement. ATP content was determined by using the Roche ATP bioluminescent assay kit HSII (Roche Applied Science) and a TD-20/20 luminometer (Turner Designs). ATP levels were normalized to total protein content.

Quantification of reactive oxygen species production. Reactive oxygen species formation was quantified as described[20,31]. Briefly, we use the membrane-permeable non-fluorescent dye 2,7-dichlorodihydrofluorescein-diacetate (H2-DCF-DA) (Sigma-Aldrich). H2-DCF-DA is deacetylated and becomes membrane impermeable after entering the cell. H2-DCF fluoresces upon oxidation to 2,7-dichlorofluorescein (DCF) by reactive oxygen species. Young adults treated as described above were washed off of the plates with M9 buffer. After washing to reduce bacterial content, a 50 μl volume of worm suspension was pipetted in four replicates into the wells of a 96-well plate with opaque walls and bottom and

allowed to equilibrate to room temperature. A fresh 100 μM H2-DCF-DA solution (50 μl) was pipetted to the suspensions, resulting in a final concentration of 50 μM. Basal fluorescence was measured after addition of H2-DCF-DA, in a microplate reader at excitation/emission wavelengths of 485 and 520 nm. Plates were kept for 1 h shaking at 20 °C. Then, a second measurement was performed. The initial fluorescence and the fluorescence signals of control wells were subtracted from the second measurement. Values were normalized to protein content.

Electrophoresis and western blot analysis. For one-dimensional SDS–PAGE, worm pellets were re-suspended in five volumes of SDS-sample buffer, boiled for 5 min, and the proteins were resolved on 15% gels. Following electrophoresis, proteins were blotted to PVDF membranes, and immunoreactive material was visualized by chemiluminescent detection (ECL; Amersham) according to the manufacturer's instructions. A polyclonal antibody raised against the 25 carboxy-terminal amino acids of the murine PHB-1 protein has been described previously[15]. Polyclonal antibody against the yeast β-subunit of F1-ATPase was a gift from J. Berden. Anti-actin antibody was obtained from ICN (clone C4) and used at a dilution of 1:10,000.

Mitochondrial DNA quantification. Mitochondrial DNA (mtDNA) was quantified using quantitative real time PCR as described previously[32]. We used the primers 5′-GTTTATGCTGCTGTAGCGTG-3′ and 5′-CTGTTAAAGCAAGTG GACGAG-3′ (Mito1 set) for mtDNA. The results were normalized to genomic DNA using the following primers specific for *ama-1*: 5′-TGGAACTCTGGA GTCACACC-3′ and 5′-CATCCTCCTTCATTGAACGG-3′. Quantitative PCR was performed using the Bio-Rad CFX96 Real-Time PCR system, and was repeated three times.

Oxygen consumption rate measurements. Oxygen consumption rates were measured as previously described[33] using a Clark-type electrode with some minor modifications (Hansatech Instruments). Young adult worms were washed and collected in S-basal buffer. Approximately 100 μl of slurry pellet of worms were delivered into the chamber in 3 ml of S-basal medium. The chamber was kept at 25 °C, and measurements were done for 5–15 min, depending on the oxygen consumption rate. The slope of the straight portion of the plot was used to derive the oxygen consumption rate. Worms were recovered after respiration measurements and collected for protein quantification. Rates were normalized to protein content. We performed three independent measurements per strain. Statistic analysis was performed using the Excel software package (Microsoft).

Membrane potential measurements. Mitochondrial membrane potential was measured *in vivo* using the fluorescent, lipophilic carbocyanine dye, 3,3′-dipropylthiacarbocyanine iodide (diS-C3(3); Sigma-Aldrich), as described[34]. Stained and washed worms were immobilized with Levamisole before mounting on 2% agarose pads for microscopic examination with a Zeiss AxioPlan microscope (Carl Zeiss) equipped with a Zeiss AxioCam digital colour camera. Images were acquired under the same exposure. Average pixel intensity values were calculated by sampling three images of different animals, three times each (nine measurements total for each strain/condition). We calculated the mean and maximum pixel intensity for each animal in these images using the ImageJ software (http://rsb.info.nih.gov/ij/). For each experiment, at least 50 images were processed over at least five independent trials.

Prohibitin overexpression. *phb-1* and *phb-2* overexpression plasmids were constructed by PCR amplification of the *phb-1* and *phb-2* loci, using primers 5′-CTCAACGCGTGAGCCATACC-3′ and 5′-CGACATCGGGGAATTGATTC-3′ for *phb-1*, and primers 5′-CGAGTCAGAGATAAAGACCG-3′ and 5′-AACCG GGAATTACATTCCAG-3′ for *phb-2*. The resulting 2.1 kb and 2.5 kb fragments for *phb-1* and *phb-2*, respectively, were inserted into the plasmid vector pCRII-TOPO (Invitrogen). The two constructs, either each alone or both, were injected into the gonads of wild-type animals, together with pPD118.33, a plasmid that carries a $p_{myo\text{-}2}$GFP reporter fusion as transformation marker (pharyngeal muscle GFP expression). pRF4, a plasmid that carries the *rol-6*(*su1006*) dominant transformation marker was also used. We have not been able to establish stable transgenic lines overexpressing either each or both prohibitin genes. Although F_1 transgenic animals expressing the co-injection marker were obtained, none of the F_1 transgenic progeny segregated *phb*-overexpressing F_2 transgenic animals, indicating that overexpression is causing lethality. Growing F_1 transgenic animals on *phb* RNAi plates (and thus quenching *phb* gene overexpression) allowed generation of F_2 transgenics. These animals stopped propagating once shifted onto regular OP50 plates.

28. Tatsuta, T., Model, K. & Langer, T. Formation of membrane-bound ring complexes by prohibitins in mitochondria. *Mol. Biol. Cell* **16,** 248–259 (2005).
29. Ashrafi, K. *et al.* Genome-wide RNAi analysis of *Caenorhabditis elegans* fat regulatory genes. *Nature* **421,** 268–272 (2003).
30. Soukas, A. A., Kane, E. A., Carr, C. E., Melo, J. A. & Ruvkun, G. Rictor/TORC2 regulates fat metabolism, feeding, growth, and life span in *Caenorhabditis elegans*. *Genes Dev.* **23,** 496–511 (2009).
31. Kampkötter, A. *et al.* Effects of the flavonoids kaempferol and fisetin on thermotolerance, oxidative stress and FoxO transcription factor DAF-16 in the model organism *Caenorhabditis elegans*. *Arch. Toxicol.* **81,** 849–858 (2007).
32. Cristina, D., Cary, M., Lunceford, A., Clarke, C. & Kenyon, C. A regulated response to impaired respiration slows behavioral rates and increases lifespan in *Caenorhabditis elegans*. *PLoS Genet.* **5,** e1000450 (2009).
33. Braeckman, B. P., Houthoofd, K., De Vreese, A. & Vanfleteren, J. R. Assaying metabolic activity in ageing *Caenorhabditis elegans*. *Mech. Ageing Dev.* **123,** 105–119 (2002).
34. Gášková, D., DeCorby, A. & Lemire, B. D. DiS-C_3(3) monitoring of *in vivo* mitochondrial membrane potential in *C. elegans*. *Biochem. Biophys. Res. Commun.* **354,** 814–819 (2007).